Open Archive Toulouse Archive Ouverte (OATAO)

This is an author's   version published in: https://oatao.univ-toulouse.fr/26597

Official URL: https://doi.org/10.1103/PhysRevE.102.011102

To cite this version :

Bauerheim, Michaël and Chapin, Vincent Route to chaos on a dragonfly wing cross section in gliding flight. (2020) Physical Review E, 102 (1). 1-6. ISSN 1539-3755

Any correspondence concerning this service should be sent to the repository administrator:
tech-oatao@listes-diff.inp-toulouse.fr

Route to chaos on a dragonfly wing cross-section in gliding flight

Michael Bauerheim[*] and Vincent Chapin[†]
ISAE-Supaéro, 10 avenue Edouard Belin,
31400 TOULOUSE (France)

The route from linear towards non-linear and chaotic aerodynamic regimes of a fixed dragonfly wing cross-section in gliding flight is investigated numerically using Direct Navier-Stokes simulations (DNS). The dragonfly wing consists in two corrugations combined with a rear arc, which is known to provide overall good aerodynamic mean performance at low Reynolds numbers. First, the three regimes (linear, non-linear and chaotic) are characterized, and validated using two different fluid solvers. In particular, a peculiar transition to chaos when changing the angle of attack is observed for both solvers: the system undergoes a sudden transition to chaos in less than $0.1°$. Second, a physical insight is given on the flow interaction between the corrugations and the rear arc, which is shown as the key phenomenon controlling the unsteady vortex dynamics and the sudden transition to chaos. Additionally, aerodynamic performances in the three regimes are given, showing that optimal performances are closely connected to the transition to chaos.

I. INTRODUCTION

The route to chaos in unsteady vortex dominated dynamics of low Reynolds number flows is of high interest for fundamentals and applications [1]. It has been first described for the flow around a cylinder by Karniadakis and Triantafyllou [2] at low Reynolds numbers where a transition to chaos occurs through a successive period-doubling associated to vortex pairing. This mechanism was then found unrealistic because of an insufficient large computational domain. Indeed, further work conducted by Henderson [3] revealed that such a transition to chaos highly depends on the computational domain size, in particular the spanwise direction: from a 2D case exhibiting a periodic state, the increase of the transverse distance leads to a quasi-periodic regime, before transitioning to chaos for large spanwise size because of two competing branches of 3D unstable modes. The transition to chaos in the flow around an inclined flat plate, however, is driven by a period-doubling and various incommensurate bifurcations associated with large flow separation [4]. The transition to chaos of the flow past a 3D blunt-based axisymmetric bluff was studied by Bury and Jardin [5] showing a succession of bifurcations associated with distinct wake patterns and symmetry breaking. The transition was refered as a Ruelle-Takens-Newhouse scenario [6], although the third frequency triggering chaos was not identified. No other chaotic regime has been reported and characterized so far for more complex fixed 2D or 3D airfoils at low Reynolds number, which is one objective of this paper. Nevertheless, more literature can be found on chaotic aerodynamics of moving objects [7, 8], where the onset of chaos is more prevalent.

On the other side, dragonfly wings are of interest for micro air vehicle (MAV) applications, which are operating in the same low Reynolds number range. The experimental study from Okamoto et al. [9] has shown that a corrugation or a sinusoidal pattern of surface roughness may be beneficial for aerodynamic characteristics. Kesel [10] also studied corrugated airfoils to understand how to reach the high maximum lift coefficient measured in wind-tunnel tests, concluding that a symmetric corrugation will not be optimal for lift generation. Vargas et al. [11] has made a CFD comparisons of a corrugated airfoil geometry from [10] with a flat plate and a profiled airfoil. A higher aerodynamic performance on lift-to-drag ratio is mentioned at the highest Reynolds number tested ($Re = 1000$) and moderate angle of attack ($\alpha = 5°$). Over a large range of Reynolds numbers [$140 - 10000$], the corrugation effect which increases lift with low drag penalty is not Reynolds number dependent [12]. Finally, numerical and experimental studies [13, 14] revealed that corrugations may also reduce the lift and drag fluctuations because of decreasing the vortex shedding magnitude. However, at lower Reynolds number, corrugations may have negative effects [15] when not accompanied by a rear arc. This scientific debate dealing with the positive and negative effects of corrugations on low-Reynolds aerodynamic performances is still open [16]. To answer this question will require more studies on the unsteady complex flow around dragonfly wings to describe in details the various regimes that can arise depending on the geometry and flow conditions. This is one motivation for the present study.

The transition from periodic to non-linear and chaotic dynamics of the flow around a dragonfly corrugated airfoil has never been studied. In particular, the possible onset of chaos and its transition route are unexplored today for such a configuration combining sharp corrugations with a smooth rear arc. Additionally, it is of high interest to better understood the underlying physics of this unsteady flow, and gives new insight for designing optimal applications in low Reynolds number flows. This is achieved in the present paper using numerical simulations

---

[*] michael.bauerheim@isae-supaero.fr
[†] vincent.chapin@isae-supaero.fr

FIG. 1. Flow configuration and geometry, detailed in [13].

of a 2D dragonfly wing exhibiting two corrugations with a rear arc (Fig. 1). First, the numerical setup is shown in Section II. Then, results on the various aerodynamic regimes are detailed in Section III, highlighting a *sudden transition to chaos* when varying the angle of attack, without the classical period-doubling or quasi-periodic states. From the authors knowledge, such an alternative and uncommon route to chaos has been reported only on mathematical non-linear systems by Chowdhury and Roychowdhury [17]. Interestingly, it is also shown that maximum lift-to-drag ratio is obtained just before the transition to chaos, whereas maximum lift is generated before leaving the chaotic state towards the non-linear regime: optimal aerodynamic performances are therefore in close connections with the transition to chaos. Finally, the vortex dynamics and flow fields are analyzed for the several regimes.

II. NUMERICAL SETUP

For this study, two different codes are used to ensure that the route towards chaos is not due to numerical errors or formulation artifacts. First, the commercial solver Fluent is used as an incompressible code with a second-order finite volume scheme in space and time. Standard Dirichlet boundary conditions are used. In complement, the legacy code from Stanford called CharlesX, now developed at ISAE-Supaero [18], is used as a fully compressible Navier-Stokes solver. A centered third-order finite volume scheme with low dissipation properties is employed. The CFL number is set to 1.2. Because of acoustic waves inherent to the compressible Navier-Stokes equations, Characteristic Boundary Conditions (CBC) are imposed at boundaries as well as a sponge zone at the outlet to further prevent acoustic wave reflections.

Thus, the present case is solved using different set of equations and numerical schemes. In both solvers, no model is used for turbulence or walls. The atmospheric pressure is imposed at the outlet, whereas velocity is imposed on the three other boundaries with value $[V_\infty \cos(\alpha), V_\infty \sin(\alpha)]$, where $V_\infty = 8.76$m/s to achieve $Re = 6000$, and α is changed from $6°$ to $10°$. Note that the kinematics of the wing is not considered here, even though it might have a significant effect on the shear layer stability, and consequently on the various regimes observed. Thus, the present study focuses only on the gliding flight mode, as already investigated

for instance by Wakeling and Ellington [19] for a dragonfly *Sympetrum sanguineum*. To limit the computational time, 2D simulations are performed, yet 3D cases have been also simulated to guarantee that chaos is still present when considering 3D effects.

The geometry is a corrugated dragonfly wing cross-section where 2 corrugations are combined with a rear arc (Fig. 1). The coordinates are provided in [13]. The chord is $c = 10$mm, and the relative thickness is $\epsilon/c = 0.5\%$. The 2D domain expands from $-10c$ to $10c$. The same mesh is used for both solvers: after a convergence study, results are presented only for a fine structured mesh containing 1.12 million quads. Close to the airfoil, the mesh is uniform with cell size $\Delta x/c = \Delta y/c = 400$.

III. RESULTS

Results for various angles of attack α are analysed to identify the aerodynamic regime depending on this parameter. Power spectrum of the lift coefficient, as well as the phase portraits based on the lift (C_L) and drag (C_D) coefficients, are displayed in Fig. 2. To ensure that the aerodynamic regimes are not artifacts of the CFD code, results are displayed for both Fluent (middle) and Charles^X (right). The frequency in the spectra are normalized by the dominant mode observed in the non-linear regime: $f_1 = 664Hz$.

For low angles of attack, corresponding to the classical *linear periodic* regime, the lift spectrum exhibits only one mode without harmonics. Its frequency shifts from $f/f_1 \approx 4$ at $7°$ toward $f/f_1 \approx 3.5$ close to the transition at $7.625°$. The phase portrait (C_L, C_D) is an ellipse repeating itself perfectly, showing that no quasi-periodic state or loss in synchronisation exist. Fluent and Charles^X agree well on this regime, especially on the frequency with a mismatch below 3%. However, a difference can be observed on the predicted amplitude (e.g. a mismatch of 13% at $7°$), with a lower amplitude for Fluent which might be due to a higher numerical dissipation. The mesh convergence revealed that the frequency and amplitude of these oscillations are very sensitive to the mesh and numerics.

When increasing the angle of attack, a sudden transition to a *chaotic state* arises. This chaos regime is also observed on coarser meshes with similar spectrum and phase portraits. The critical angle of attack is evaluated at $\alpha_c = 7.7°$ in Fluent. Using Charles^X, the transition is slightly delayed to higher angles. 3D simulations have been also conducted, and confirm the transition to chaos when 3D effects are taken into account. This chaos is characterized by broadband spectra and complex phase portraits. After the transition, the oscillations have large amplitudes and show no synchronisation between the lift and drag forces. Compared to the transition to chaos observed for a fixed flat plate [4], which arises at large angle of attack ($\alpha_c \approx 20 - 25°$) because of the flow separation, here the transition occurs at low angle of attack
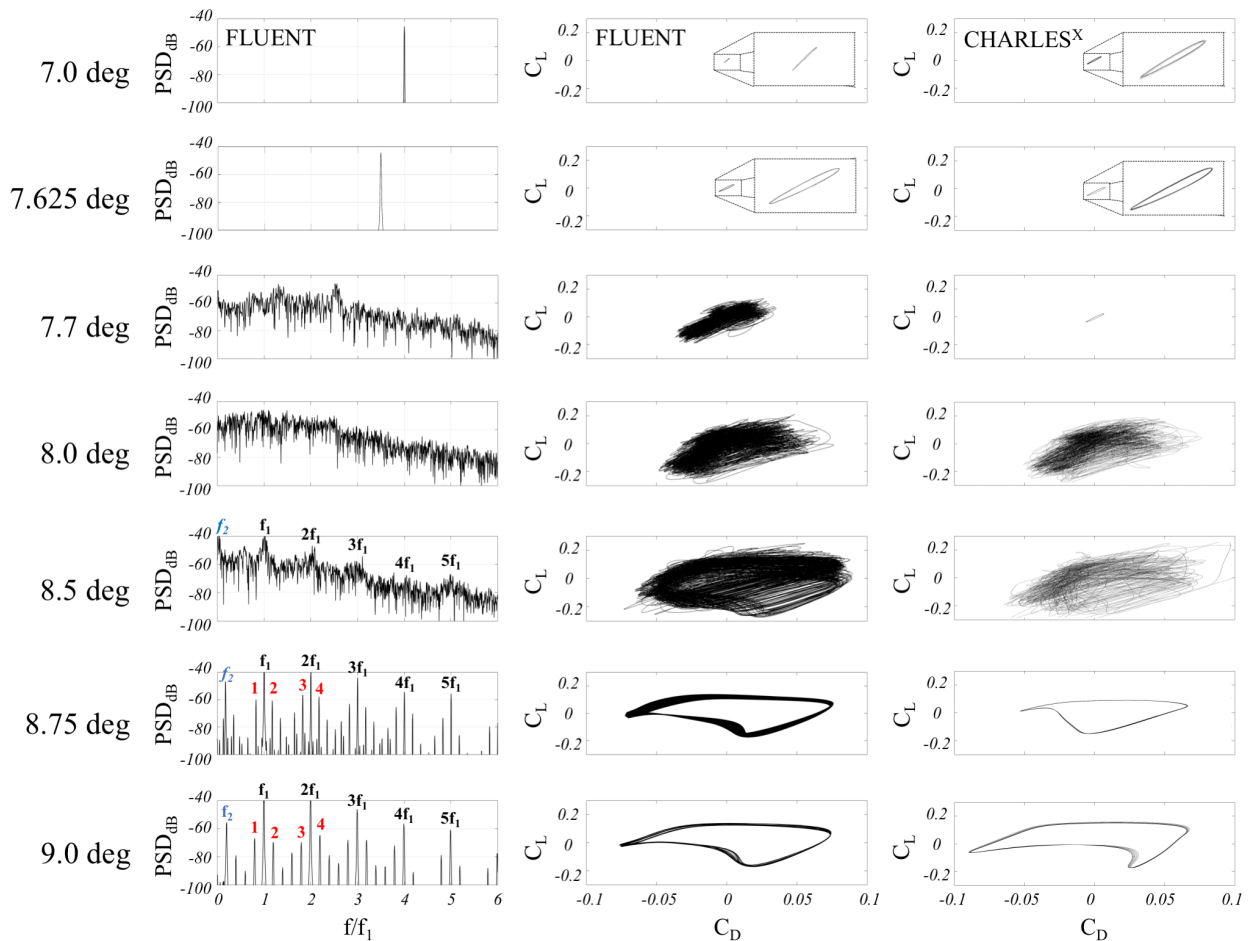
FIG. 2. Power spectrum density of the lift (left, Fluent), and phase portrait (C_L,C_D) for several angles of attack α obtained by Fluent (middle) and CharlesX (right).

($\alpha_c \approx 7.7°$). Interestingly, no period-doubling or quasi-periodic state appears before the transition: it occurs suddenly from a pure periodic regime to a chaotic state when increasing the angle of attack of $\Delta\alpha = 0.075°$. Such a transition has not been reported yet in the literature in an aerodynamic context. Based on the phase portrait at 8° and 8.5°, Fluent and Charles^X agree well on this chaotic regime.

Then, another periodic situation occurs for larger angles of attack, here displayed for $\alpha > 8.5°$. Compared to the *linear periodic* case, here the phase portraits are no more ellipses. This is due to a non-linearity and the presence of multiple harmonics nf_1, where n is an integer and $f_1 = 664$Hz is the fundamental harmonics of the mode. This situation is known as non-linear periodic oscillations. Again, both solvers agree well on both the pattern and amplitude. Note that compare to the linear regime where the frequency of the dominant mode was drifting when increasing the angle of attack, here the frequency f_1 does not depend on α. Additionally, a new mode at frequency $f_2 \approx 115Hz$ appears (denoted in blue in Fig. 2), which is not an harmonics of f_1: this is

an incommensurate frequency, where $f_1/f_2 = 5.47$. This mode f_2 interacts non-linearly with the dominant mode f_1, leading to numerous interaction modes (denoted in red) with frequencies $nf_1 + pf_2$, where n and p are integers. For example, the mode 1 is $f_1 - f_2$, and the mode 2 is $f_1 + f_2$. Because of their low amplitudes, these modes are not visible on the phase portraits which are driven by the dominant mode f_1 and its harmonics nf_1. Note that the modes associated with f_2 do not appear on coarser meshes, yet a similar dynamics of the system is observed. It suggests that the mode f_2 does not play a significant role in the onset of chaos and its transition to the non-linear regime.

The route through the chaotic state, from the linear to the non-linear periodic regimes, is investigated further by analyzing simulations for angles of attack from 7° to 9.5°. Figure 3 displays both the mean aerodynamic performances (top) and the frequency content depending on the angle of attack. The frequency content is extracted by computing the Fourier transform of the lift fluctuations. A threshold is then applied to keep only relevant frequencies, here set to 10% of the main peaks ($\bullet$). The

dominant modes are highlighted by ● corresponding to a threshold set to 95%. Thus, each ● (dominant modes) and ● (other modes) in Fig. 3 (bottom) corresponds to one relevant frequency in the spectrum. As in Fig. 2, three regimes are observed: (i) the *linear periodic* regime dominated by one single mode, (ii) a *chaotic state* with a broadband spectrum with numerous relevant modes, and (iii) the *non-linear periodic* oscillations dominated by f_1 and its harmonics. Note that for this regime, a second incommensurate mode appears at f_2. Since its amplitude is low, this regime is not dominated by the pair (f_1, f_2) but rather by $(f_1, 2f_1)$: this regime is therefore described as *non-linear periodic* rather than *quasi-periodic*. It also reveals the sudden transition to chaos at $\alpha_c \approx 7.7°$. During this transition, it is found that the dominant mode at $f \approx 2200Hz$ keeps on drifting throughout the chaotic state towards the null frequency at $\alpha = 8.5°$ (denoted f_0 in Fig. 2, $\alpha = 8.5°$). Meanwhile, the mode f_1 appears with a locked frequency independent of the angle of attack, also visible in Fig. 2. The transition when leaving the chaos to the non-linear regime is however smooth, with a broadband content diminishing with α. The main features characterizing the chaotic state is its sudden transition to chaos and the frequency drift towards the null frequency, highlighted by the decreasing dashed line in Fig 3. This is in contrast with the gradual transition to chaos observed on a fixed flat plate at large angles of attack and lower Reynolds number [4], since here the system enters suddenly into the chaotic state [7.625°, 7.70°] without noticeable period doubling, quasi-periodic state, or intermittency. This alternative route to chaos has been reported by Awrejcewicz [20] as well as Chowdhury and Roychowdhury [17] for non-linear oscillators forced with static and fluctuating loads. For practical applications such as drones, identifying precursors to avoid this sudden entrance into chaos will be challenging.

In complement, Fig. 3 also displays the evolution of the aerodynamic performances C_L (●) and C_D (■) when changing α. The mean lift-to-drag ratio is also displayed (♦). Both mean coefficients (in black) and fluctuations (in red) are shown. The *linear periodic regime* is characterized by a high lift-to-drag ratio due to a high lift and low drag. This performance increases with the angle of attack due to the higher lift, leading to a maximum lift-to-drag ratio $\bar{C}_L/\bar{C}_D = 13.6$ close to the transition at $\alpha = 7.625°$. This regime also exhibits low RMS value for the aerodynamic coefficients, as expected from Fig. 2. In the *chaotic state*, the lift coefficient is still increasing rapidly, leading to a maximum $C_L = 1.19$ at $\alpha \approx 8.5$, which corresponds to a gain of 33% compared to the linear regime. This high lift capability is accompanied by a large increase of drag and fluctuation levels, resulting in lower lift-to-drag ratio. Thus, the high lift mechanism might be due to the generation of an intense vortex dynamics that acts as a circulatory force (vortex-induced lift), known to be an efficient lift generation in unsteady low Reynolds number flows [21]. A further analysis of
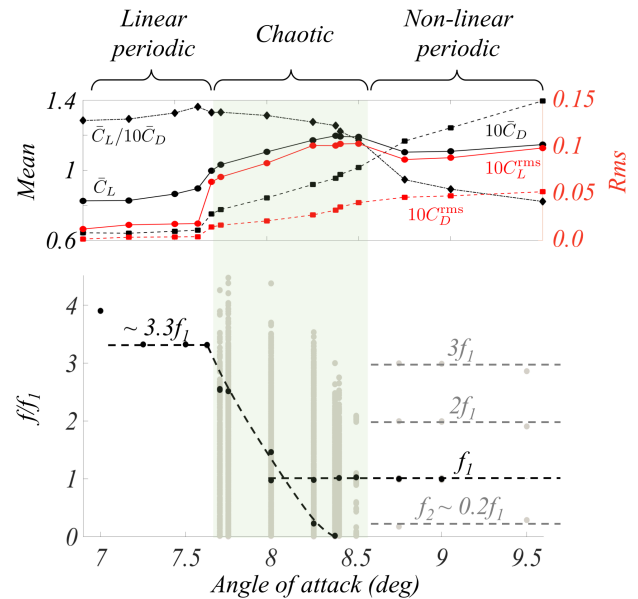

FIG. 3. Mean ($\bar{C}_L$, $10\bar{C}_D$ and $\bar{C}_L/10\bar{C}_D$) and RMS (C_L^{rms} and C_D^{rms}) aerodynamic performances (top) as well as frequency content f/f_1 (bottom) depending on the angle of attack α obtained by Fluent. The chaotic regime is highlighted in green. Frequency values and trends (dashed lines) are also displayed (black for the main mode, gray for harmonics).

the flow field is proposed in the following to validate this assumption. Finally, in the non-linear regime, the lift coefficient is still large ($C_L \approx 1.1$) but with large oscillations and extreme drag penalties. Interestingly, Fig. 3 reveals that the *chaotic state* is tightly connected to the optimal performance of the dragonfly wing: the maximum lift-to-drag ratio is obtained just before the transition to chaos, whereas the maximum lift coefficient is reached before leaving the chaos towards the non-linear regime. Thus, understanding the transitions to chaos and their underlying physics is of key interest to propose optimal wing designs at low Reynolds numbers.

To understand the physics governing the transition to chaos, the flow fields obtained in the three regimes are displayed in Fig. 4 for $\alpha = 7°$ (*linear periodic*), $\alpha = 8°$ (*chaos*), and $\alpha = 9°$ (*non-linear periodic*). In the first periodic regime, for $\alpha < \alpha_c = 7.7°$, the vortex dynamics is dominated by the trailing-edge vortex (P_{TEV}^+) emitted from the pressure side at frequency $f = 2100Hz - 2600Hz$ depending on α. The suction side shear layer is not sufficiently unstable to generate vortices, but small perturbations due to Kelvin-Helmholtz instability (S_{KH}^-) can be observed with m=3 perturbations along the chord, locked at the TEV's frequency.

In the chaotic regime (here displayed for $\alpha = 8°$), the shear layer developing at the suction side generates $m = 3$ vortices (S_{KH}^-) with partial pairing along the rear arc. Hence, the vortex intensity is higher, explaining the higher lift and drag fluctuations observed in Fig. 3. These large vortices induce a reverse flow on the suction
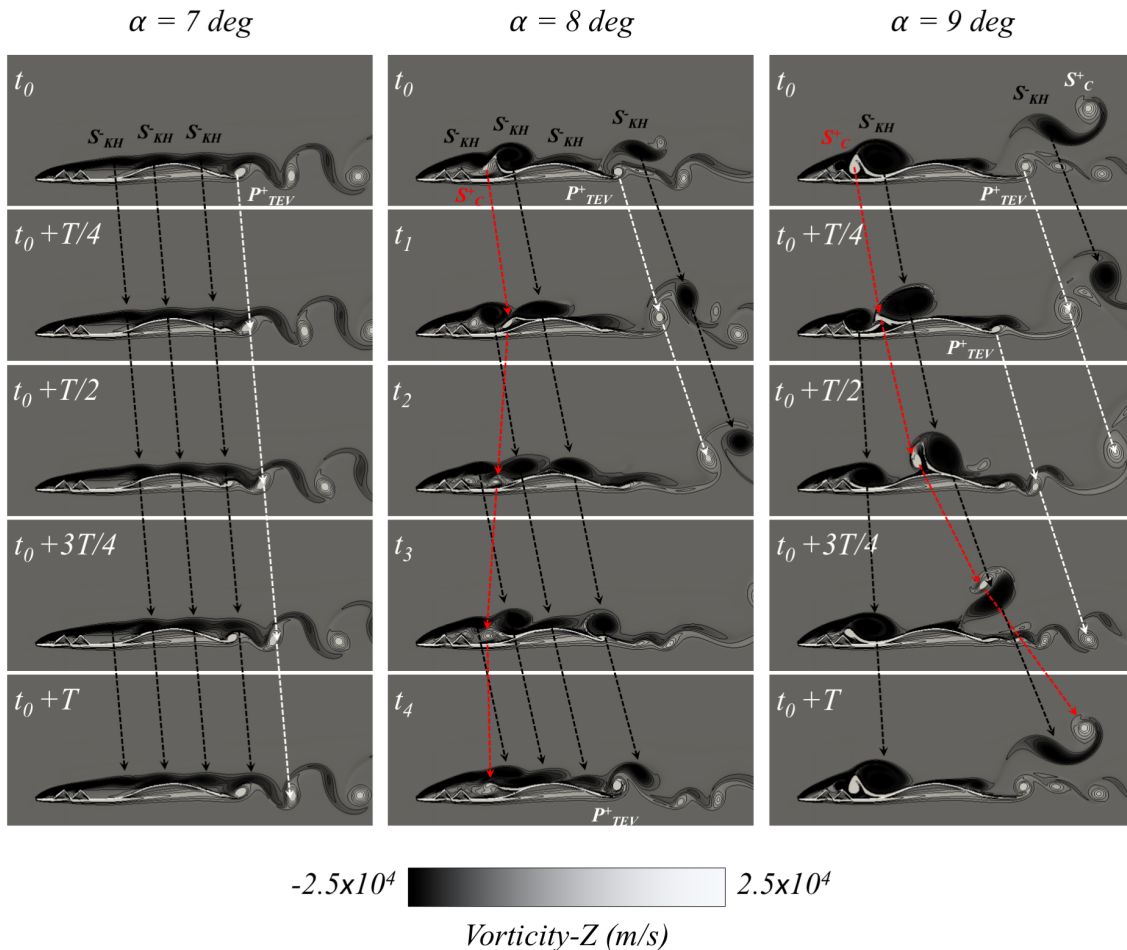
FIG. 4. Five instantaneous vorticity fields and contours for the three angles of attack obtained by CharlesX: $\alpha = 7°$ (linear), $8°$ (chaotic), and $9°$ (non linear). Arrows allows the tracking of vortices in time, revealing their associated dynamics.

side of the rear arc, highlighted by a positive vortex sheet (S_C^+) with a complex dynamics (red arrows) not yet fully developed. One hypothesis of the occurrence of chaos is the competitive interaction between modes from the main and reverse flows in the cavity between the second corrugation and the rear arc as described by Ciliberto and Gollub [22]. In the wake, the S_{KH}^- vortex interacts with the smaller P_{TEV}^+ shed at the pressure side creating a vortex dipole of opposite sign with fluid ejection on the upper side. It can be noticed on the fourth snapshot at $8°$ that the chaotic state can leads to *silences* due to the intermittent damping of lift and drag oscillations. In such *silences*, also observed by Bury and Jardin [5] in a 3D bluff body case at low Reynolds numbers ($R_e = 900$), the wake is almost steady, which may open the path to non-linear control strategies to benefit from the large lift coefficient obtained in the chaotic state but with low oscillations of aerodynamic coefficients.

In the third non-linear periodic regime (here displayed for $\alpha = 9°$), the shear layer at the suction side is more unstable. It sheds higher magnitude vortices with multiple pairing (S_{KH}^- and positive vortex S_C^+) in the cavity between second corrugation and rear arc, with $m = 2$. The reverse flow inducing the S_C^+ is also more intense, and its dynamics is now locked with the S_{KH}^- instability forming a vortex dipole of opposite sign. This dipole is convected downstream on the upper side before reaching the rear arc where the TEV vortex (P_{TEV}^+) is generated at trailing-edge on the lower side. Later, the two vortices of the dipole (S_{KH}^- and S_C^+) eject fluid on the upper side before being separated downstream in the wake. Further downstream, not shown here, S_{KH}^- interacts with the P_{TEV}^+ in the far wake. Note that the mode f_2 is difficult to identify in the physical space because appearing at a larger time-scale with low amplitude.

IV. CONCLUSION

The evolution of the aerodynamic regimes of a fixed dragonfly wing at low Reynolds number ($R_e = 6000$) has been investigated using Direct Navier-Stokes simulations (DNS). The dragonfly wing section consists in two corrugations followed by a rear arc, which is known to provide overall good aerodynamic performances at low Reynolds numbers. When increasing the angle of attack, a sudden transition to chaos appears. It is due to the complex interaction between the main unstable shear layer produced at the leading-edge and an induced reverse flow in the cavity between the second corrugation and the rear arc on the suction side. For higher angles of attack, a non-linear periodic regime is observed. Interestingly, optimal performances of the dragonfly wing are connected with this transition to chaos: the maximum lift-to-drag ratio is obtained just before the transition, whereas the highest lift coefficient is reached when leaving the chaotic state towards the non-linear regime. Moreover, in the chaotic regime, silence associated with the intermittent damping of the lift and drag fluctuations leads to an almost steady wake with a high lift coefficient. It suggests that optimal wing designs and control strategies could be achieved for profiles with both corrugations and a rear arc. When focusing on the flow fields and vortex dynamics, numerical simulations reveal that the reverse flow between the corrugation and the rear arc seem of a crucial interest, probably controlling the transitions to chaos and the non-linear regime. This paper highlights that the flow in such corrugated configuration is complex, and still requires further works to better understand its dynamics and evolution with the flight conditions.

[1] S. Ho, H. Nassel, N. Pornsinsiriak, and Y.-C. Tai, Progress in Aerospace Science **39**, 635 (2003).

[2] G. Karniadakis and G. Triantafyllou, J. Fluid Mech. **238**, 1 (1992).

[3] R. Henderson, J. Fluid Mech. **352**, 65 (1997).

[4] J. Zhang, N.-S. Liu, and X.-Y. Lu, Physical Review E **79** (2009).

[5] Y. Bury and T. Jardin, Physics Letter A **376**, 3219 (2012).

[6] J. P. Eckmann, Rev. Mod. Phys. **53**, 643 (1981).

[7] P. G. Perdikaris, L. Kaiktsis, and G. S. Triantafyllou, Physics of Fluids **21**, 101705 (2009).

[8] C. Bose and S. Sarkar, Physics of Fluids **30**, 047101 (2018).

[9] M. Okamoto, K. Yasuda, and A. Azuma, Journal of experimental biology **199**, 281 (1996).

[10] B. Kesel, The Journal of experimental biology **203**, 3125 (2000).

[11] A. Vargas, R. Mittal, and H. Dong, Bioinspiration and biometics **3**, 026004 (2008).

[12] W.-K. Kim, J. H. Ko, H. C. Park, and D. Byun, Journal of theoretical biology **260**, 523 (2009).

[13] D.-E. Levy and A. Seifert, Physics of fluids **21** (2009).

[14] D.-E. Levy and A. Seifert, Journal of theoretical biology **266**, 691 (2010).

[15] X. G. Meng and M. Sun, Physics of Fluids **25**, 071905 (2013).

[16] Y. Chen and M. Skote, Journal of Fluids and Structures **62**, 1 (2016).

[17] K. Chowdhury and R. Roychowdhury, Chaos, Solitons & Fractals **4**, 2057 (1994).

[18] R. Lamouroux, J. Gressier, and G. Grondin, Journal of Scientific Computing **67**, 375 (2016).

[19] J. Wakeling and C. Ellington, Journal of experimental biology **200**, 543 (1997).

[20] J. Awrejcewicz, Journal of the Physical Society of Japan **58**, 4261 (1989).

[21] T. Jardin, N. Doué, S. Prothin, and J.-M. Moschetta, Journal of Fluids and Structures **62** (2016).

[22] S. Ciliberto and J. P. Gollub, Phys. Rev. Lett. **52**, 922 (1984).